Published Online: 18 October, 2018 | Supp Info: http://doi.org/10.1084/jem.20170852
Downloaded from jem.rupress.org on October 25, 2018

JEM Journal of Experimental Medicine

BRIEF DEFINITIVE REPORT

A20-binding inhibitor of NF-κB (ABIN) 2 negatively regulates allergic airway inflammation

Sonia Ventura[1*], Florencia Cano[1*], Yashaswini Kannan[1*], Felix Breyer[1], Michael J. Pattison[1], Mark S. Wilson[3], and Steven C. Ley[2]

TPL-2 MAP 3-kinase promotes inflammation in numerous mouse disease models and is an attractive anti-inflammatory drug target. However, TPL-2–deficient (*Map3k8*$^{-/-}$) mice develop exacerbated allergic airway inflammation to house dust mite (HDM) compared with wild type controls. Here, we show that *Map3k8*$^{D270A/D270A}$ mice expressing kinase dead TPL-2 had an unaltered response to HDM, indicating that the severe airway inflammation observed in *Map3k8*$^{-/-}$ mice is not due to blockade of TPL-2 signaling and rather reflects a TPL-2 adaptor function. Severe allergic inflammation in TPL-2–deficient mice was likely due to reduced levels of ABIN-2 (TNIP2), whose stability depends on TPL-2 expression. *Tnip2*^{E256K} knock-in mutation, which reduced ABIN-2 binding to A20, augmented the HDM-induced airway inflammation, but did not affect TPL-2 expression or signaling. These results identify ABIN-2 as a novel negative regulator of allergic airway responses and importantly indicate that TPL-2 inhibitors would not have unwanted allergic comorbidities.

Introduction

The MAP-3 Kinase Tumor Progression Locus 2 (TPL-2; also known as MAP3K8 and COT) is a key regulator of inflammation. Following TLR and TNFR1 stimulation of myeloid cells, TPL-2 phosphorylates and activates MKK1/2 and MKK3/6, leading to the activation of the downstream ERK1/2 and p38α MAP kinases, respectively, and modulation of inflammatory cytokine and chemokine production (Gantke et al., 2011, 2012; Pattison et al., 2016).

TPL-2 promotes inflammation in numerous disease models, including endotoxic shock, experimental autoimmune encephalomyelitis, inflammatory bowel disease, pancreatitis, liver fibrosis, and thrombocytopenia (Gantke et al., 2012; Sriskantharajah et al., 2014; Xiao et al., 2014). Consequently, TPL-2 is considered an attractive anti-inflammatory drug target (George and Salmeron, 2009). However, TPL-2–deficient (*Map3k8*$^{-/-}$) mice develop more severe type 2 allergic airway inflammation in response to challenge with ovalbumin or house dust mite (HDM; Watford et al., 2010; Kannan et al., 2016). TPL-2 inhibitors, therefore, could have unwanted impacts on allergic comorbidities.

In the present study, we directly tested the effect of inhibiting TPL-2 catalytic activity in HDM allergic responses using mice that express kinase-inactive TPL-2 (*Map3k8*$^{D270A/D270A}$; Sriskantharajah et al., 2014). Surprisingly, we found that the HDM-induced allergic response was not altered by *Map3k8*^{D270A} mutation, indicating that the severe airway inflammation observed in *Map3k8*$^{-/-}$ mice compared with WT controls is not due to a blockade of TPL-2 signaling and rather reflects an adaptor function of TPL-2.

In unstimulated cells, TPL-2 forms a ternary complex with NF-κB1 p105 and A20 binding inhibitor of NF-κB 2 (ABIN-2; also known as TNIP2), a ubiquitin binding protein (Gantke et al., 2012). We have recently found that *Map3k8*$^{-/-}$ cells are profoundly deficient in ABIN-2, while *Map3k8*$^{D270A/D270A}$ cells have normal levels of TPL-2 and ABIN-2 (Sriskantharajah et al., 2014). Reduced levels of ABIN-2 therefore may contribute to the severe allergy phenotype in *Map3k8*$^{-/-}$ mice. Consistent with this hypothesis, *Tnip2*^{E256K} knock-in mutation augmented the airway allergic response to HDM by reducing ABIN-2 binding to A20 (Dong et al., 2011), a key negative regulator of inflammation (Catrysse et al., 2014). *Tnip2*^{E256K} mutation did not affect TPL-2 protein expression or TPL-2 activation of ERK1/2.

Our results identify a novel contribution for ABIN-2 in Th2-mediated inflammation and question the validity of using *Map3k8*$^{-/-}$ mice to investigate the roles of TPL-2 in disease models. Importantly, our study also implies that the use of TPL-2 inhibitors to treat inflammatory diseases would not promote allergic airway responses.

[1]The Francis Crick Institute, London, England, UK; [2]Department of Medicine, Imperial College London, London, England UK; [3]Immunology Discovery, Genentech Inc., South San Francisco, CA.

*S. Ventura, F. Cano, and Y. Kannan contributed equally to this paper; Correspondence to Steve Ley: sley@imperial.ac.uk; Mark S. Wilson: wilson.mark@gene.com.

© 2018 Ventura et al. This article is distributed under the terms of an Attribution–Noncommercial–Share Alike–No Mirror Sites license for the first six months after the publication date (see http://www.rupress.org/terms/). After six months it is available under a Creative Commons License (Attribution–Noncommercial–Share Alike 4.0 International license, as described at https://creativecommons.org/licenses/by-nc-sa/4.0/).

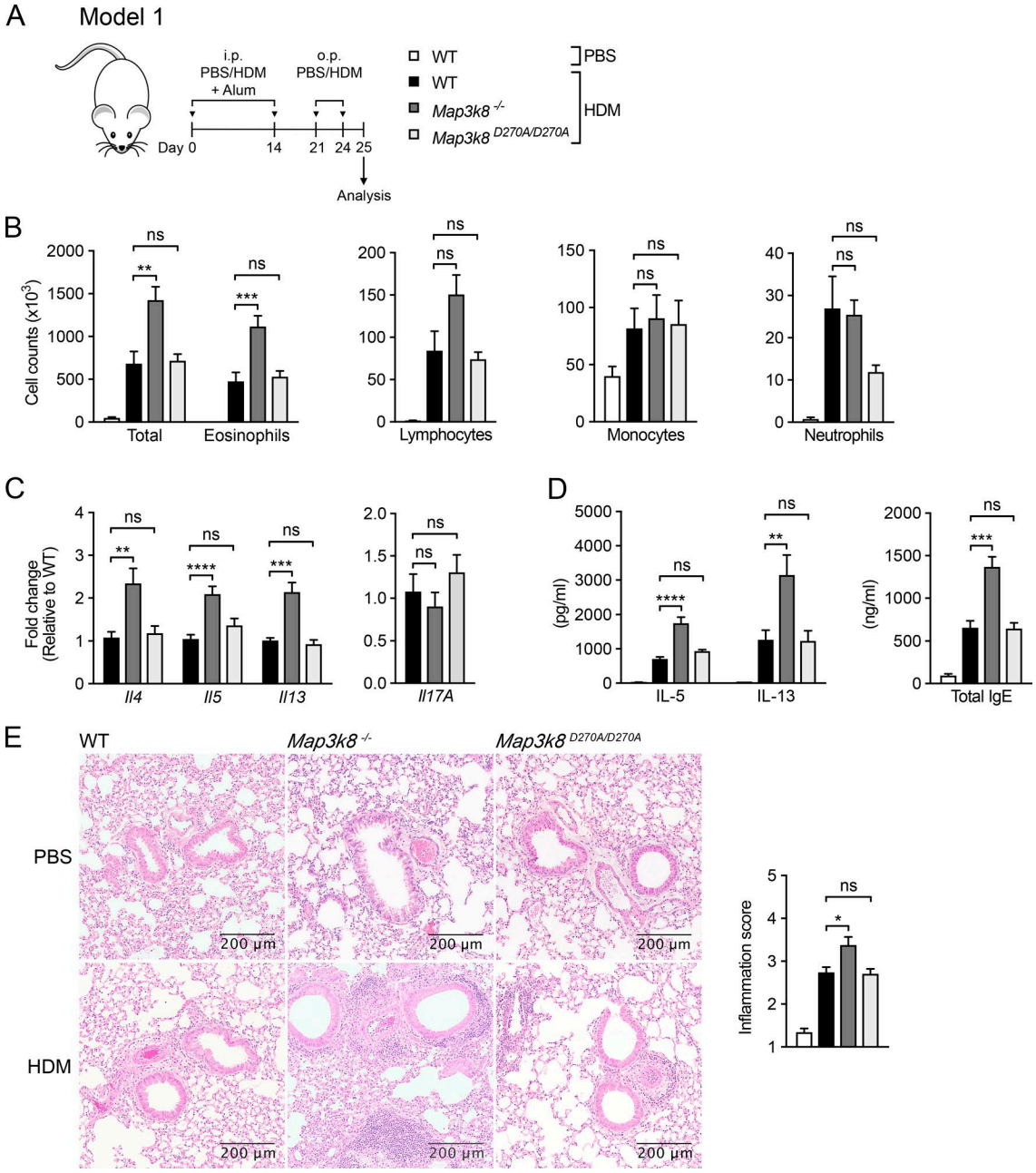

Figure 1. ***Map3k8$^{D270A/D270A}$* mice do not develop an exacerbated HDM-induced allergic response. (A)** Schematic representation of HDM/Alum-dependent allergy model (Model 1). o.p., oropharyngeal. **(B)** Differential cell counts in BAL fluids of PBS- and HDM-challenged WT, *Map3k8*$^{-/-}$, and *Map3k8*$^{D270A/D270A}$ mice. **(C)** Cytokine mRNA expression levels in the lung, as assessed by qRT-PCR. **(D)** Total IgE levels in blood serum, IL-5, and IL-13 levels in BAL fluid, as assessed by ELISA. **(E)** H&E-stained lung sections (left) and inflammation scores (right). Data in panels A–E are shown as mean ± SEM and are pooled from three independent experiments (n = 14 mice/genotype). *, P < 0.05; **, P < 0.005; ***, P < 0.001; ****, P < 0.0001. Comparisons assessed by Kruskal-Wallis and Dunn-Bonferroni's post hoc test. ns, not significant.

Results and discussion

TPL-2 kinase activity does not exacerbate the allergic response to HDM

We have recently shown a role for TPL-2 in restricting type 2 immune responses in a mouse model of allergic asthma, based on the analysis of *Map3k8*$^{-/-}$ mice (Kannan et al., 2016). Intraperitoneal sensitization with Alum and HDM followed by localized airway challenge with HDM is a well-established CD4^{+} T cell–dependent model of allergy (Haspeslagh et al., 2017). Using this model (Model 1; Fig. 1 A), we demonstrated previously that TPL-2 deficiency in *Map3k8*$^{-/-}$ mice leads to severe HDM-induced airway inflammation, with increased eosinophilia and peribronchovascular infiltrates relative to WT controls (Kannan et al., 2016). To further characterize the role of TPL-2 in allergic responses to HDM, we then tested the requirement for its kinase activity, using mice homozygous for a mutation that renders TPL-2 catalytically inactive (*Map3K8*^{D270A}; Sriskantharajah et al., 2014; Pattison et al., 2016).

Distinct from *Map3k8*$^{-/-}$ mice, which developed a severe allergic response to HDM as expected (Kannan et al., 2016), the response of *Map3k8*$^{D270A/D270A}$ mice was similar to WT controls (Fig. 1). 1 d after the final oropharyngeal HDM challenge, *Map3K8*$^{D270A/D270A}$ mice had similar cellular infiltration in bronchoalveolar lavage (BAL) fluid as WT mice (Fig. 1 B). Equivalent inflammatory responses were also detected measuring the levels of inflammatory cytokines in the lung (mRNA) and BAL fluid (protein; Fig. 1, C and D) and serum total IgE (Fig. 1 D), a hallmark in allergic responses. Consistent with these results, and in contrast to TPL-2–deficient mice, we also observed no significant differences in peribronchial and perivascular inflammation or changes in lung architecture between HDM-challenged *Map3k8*$^{D270A/D270A}$ mice and WT controls (Fig. 1 E).

Previous work from our laboratory has ruled out T cell– and B cell–intrinsic requirements for TPL-2 in HDM-induced allergy. Rather, we found an essential role for TPL-2 in dendritic cells (DCs) in limiting severe airway inflammation (Kannan et al., 2016). We therefore tested if there was a DC-intrinsic role for TPL-2 kinase activity using an allergy model (Model 2; Fig. 2 A) with adoptively transferred HDM-pulsed bone marrow–derived DCs (BMDCs; Lambrecht et al., 2000). Consistent with results obtained using the HDM-induced allergy model in intact mice, *Map3k8*^{D270A} mutation did not alter the allergic response to oropharyngeal HDM after adoptive transfer of HDM-pulsed BMDCs (Fig. 2, B–E). Recipients of *Map3k8*$^{D270A/D270A}$ and WT HDM-pulsed BMDCs showed comparable levels of cellular infiltration in BAL fluid (Fig. 2 B), inflammatory cytokine levels in the lung (mRNA; Fig. 2 C) and BAL fluid (protein; Fig. 2 D), IgE levels in serum (Fig. 2 D), and lung inflammation (Fig. 2 E). These results are in contrast to the more severe allergic phenotypes observed in recipients of *Map3k8*$^{-/-}$ BMDC (Fig. 2, B–E), consistent with previous experiments (Kannan et al., 2016).

Our earlier experiments with *Map3k8*$^{D270A/D270A}$ mice demonstrated that TPL-2 catalytic activity promotes the development of experimental autoimmune encephalomyelitis (EAE), a model of central nervous system inflammation and multiple sclerosis (Sriskantharajah et al., 2014). In contrast, the results in this section showed that TPL-2 catalytic activity did not regulate airway allergic responses to HDM in intact mice. These results imply that the severe airway inflammation that develops in *Map3k8*$^{-/-}$ mice is not due to a blockade of TPL-2 kinase signaling, but may result from the absence of TPL-2 scaffolding function.

Map3k8$^{-/-}$ mice have been used widely to investigate the role of TPL-2 in several autoimmune and inflammatory disease models (Gantke et al., 2012). Based on the largely suppressive effects of TPL-2 deficiency on inflammation in such studies, it has been concluded that TPL-2 is a good anti-inflammatory drug target and several pharmaceutical companies have developed small molecule inhibitors of TPL-2 (George and Salmeron, 2009; Gutmann et al., 2015). The results of the present study raise the possibility that some of the phenotypes detected *Map3k8*$^{-/-}$ mice in such models are actually caused by blocking ABIN-2, and not TPL-2 signaling. It will be important in future disease model studies to use *Map3k8*$^{D270A/D270A}$ mice, in which TPL-2 signaling is prevented without affecting steady-state levels of ABIN-2, to assess the potential therapeutic effects of small molecule TPL-2 inhibitors.

Tnip2 null mutation phenocopies Map3k8-null mutation in HDM-induced allergy

We have previously shown that ABIN-2 protein stability is dependent on TPL-2 expression in macrophages (Papoutsopoulou et al., 2006; Sriskantharajah et al., 2014). Therefore, one possible explanation for the difference in the phenotypes observed between *Map3k8*$^{-/-}$ and *Map3k8*$^{D270A/D270A}$ mice in the HDM allergy model was that only the former were deficient in ABIN-2 (Sriskantharajah et al., 2014). This suggests that reduced levels of ABIN-2 in DCs might have contributed to the severe allergy phenotype in TPL-2–deficient mice. Consistent with this hypothesis, TPL-2 expression, but not TPL-2 catalytic activity, was required to stabilize ABIN-2 in BMDCs (Fig. S1 A). Furthermore, *Tnip2*$^{-/-}$ mice, which lack ABIN-2 expression (Papoutsopoulou et al., 2006), displayed significantly increased lung inflammation following HDM challenge (Model 1), similar to *Map3k8*$^{-/-}$ mice (Fig. S1 C). Compared with WT controls, *Tnip2*$^{-/-}$ mice had elevated numbers of total cells and eosinophils in the BAL fluid (Fig. S1 D), higher levels of Th2 cytokine protein in BAL fluid (Fig. S1 E) and Th2 cytokines mRNAs in the lung (Fig. S1 F), and increased serum total IgE (Fig. S1 G). Similarly, adoptive transfer of HDM-pulsed *Tnip2*$^{-/-}$ BMDCs into C57BL/6J recipients (Model 2) augmented pulmonary inflammation compared with WT BMDC transfer following HDM challenge (Fig. S1 I). ABIN-2 deficiency in BMDCs also significantly increased infiltration of total cells and eosinophils in BAL fluid (Fig. S1 J), increased *Il4* and *Il13* mRNA levels in BAL fluid (Fig. S1 K) and Th2 cytokine mRNA expression in the lung (Fig. S1 L), and augmented serum IgE (Fig. S1 M).

The results in this section demonstrate that *Tnip2* deletion in intact mouse and BMDC transfer models increased the airway allergic response to HDM, similar to *Map3k8* deletion (Kannan et al., 2016). However, since ABIN-2 is required to stabilize TPL-2 protein (Papoutsopoulou et al., 2006) and *Tnip2*$^{-/-}$ BMDCs have very low levels of TPL-2 (Fig. S1 A), it was not possible to conclude from these experiments that negative regulation of HDM allergic responses was mediated by ABIN-2 itself and not another putative TPL-2–associated protein.

TNIP2^{E255K} mutation specifically reduces ABIN-2 binding to A20

Genetic polymorphisms in *TNFAIP3*, the gene encoding the negative regulator of inflammation A20, are associated with risk of asthma and allergies (Li et al., 2012; Schuijs et al., 2015). Furthermore, analyses of A20 conditional knockout mice have demonstrated that A20 expression in lung epithelial cells, myeloid cells, and DCs is required to suppress HDM-induced allergic airway inflammation (Vroman et al., 2018). ABIN-2 was originally identified by virtue of its ability to bind to A20 (Van Huffel et al., 2001). The results of the present study raised the possibility that binding to ABIN-2 might be required to mediate the inhibitory function of A20 in HDM allergic responses.

Inactivating somatic mutations in *TNIP2* are found in the activated B cell subtype of diffuse large B cell lymphoma (gastrointestinal diffused large B cell lymphoma; Dong et al., 2011). One of these mutations, *TNIP2*^{E255K}, has been shown to impair binding

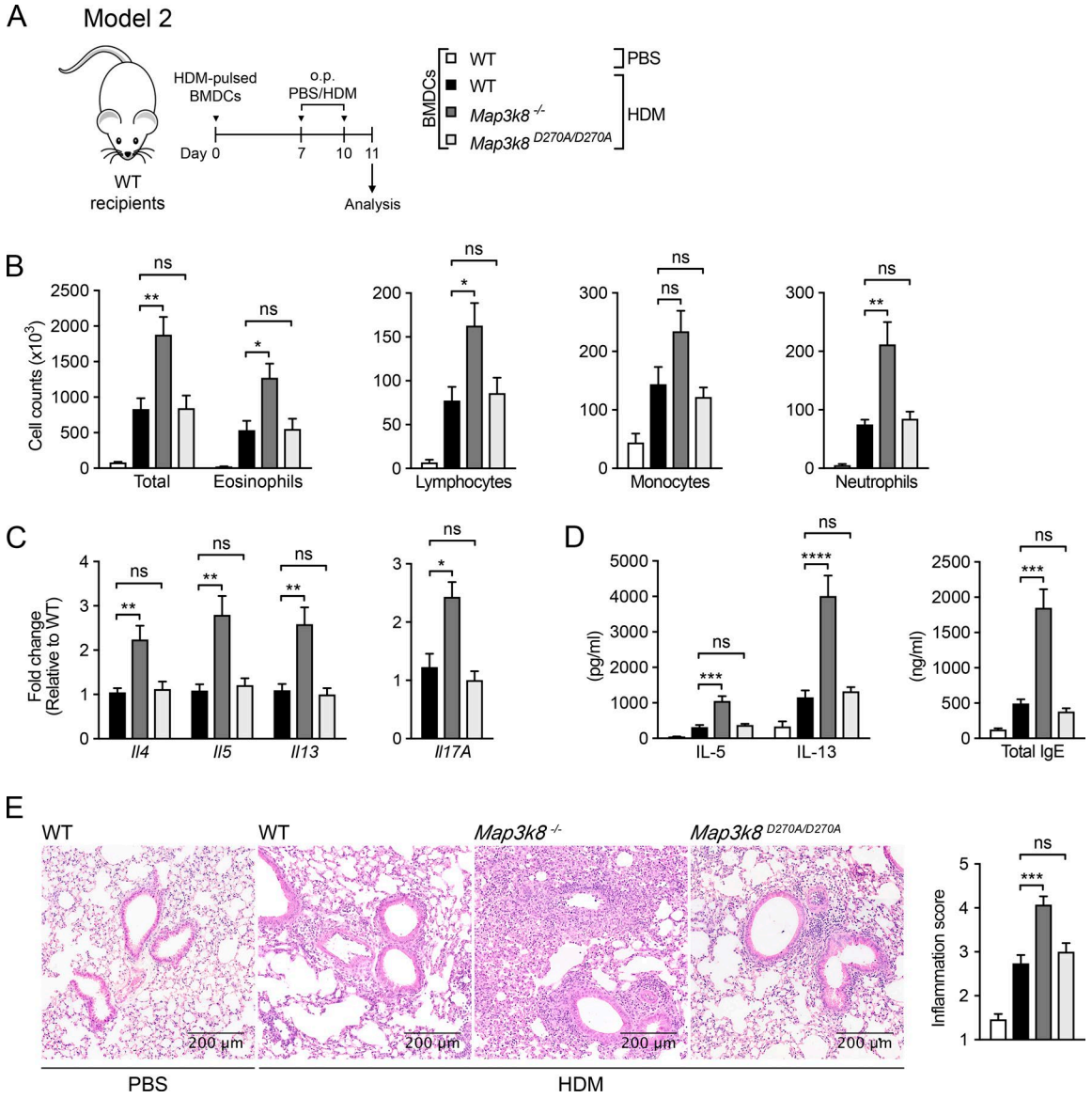

Figure 2. **HDM-pulsed *Map3k8*$^{D270A/D270A}$ BMDCs fail to induce a severe airway allergic response. (A)** Schematic representation of the BMDC adoptive transfer model of HDM-induced airway allergic inflammation (Model 2). o.p., oropharyngeal. **(B)** Differential cell counts in BAL fluids of PBS and HDM-challenged WT mice after adoptive transfer of HDM-pulsed WT, *Map3k8*$^{-/-}$, or *Map3k8*$^{D270A/D270A}$ BMDCs. **(C)** Cytokines mRNA expression levels in the lung, as assessed by qRT-PCR. **(D)** Total IgE levels in blood serum, IL-5, and IL-13 levels in BAL fluid, as assessed by ELISA. **(E)** H&E-stained lung sections (left) and inflammation scores (right). Data in panels B–E are shown as mean ± SEM and are pooled from three independent experiments (n = 12–13 mice/genotype). *, P < 0.05; **, P < 0.005; ***, P < 0.001; ****, P < 0.0001. Comparisons assessed by Kruskal-Wallis and Dunn-Bonferroni's post hoc test. ns, not significant.

of A20 to ABIN-2, based on coimmunoprecipitation experiments. However, the potential effect of *TNIP2*^{E255K} mutation on ABIN-2 binding to other known interactors was not tested. Consequently, it remained unclear whether *TNIP2*^{E255K} mutation specifically impaired ABIN-2–A20 interaction.

The effects of *TNIP2*^{E255K} mutation on established ABIN-2 interactions (shown schematically in Fig. 3 A; Lang et al., 2004; Wagner et al., 2008; Banks et al., 2016) were determined in GST pulldown experiments. GST-ABIN-2^{E255K} bound to TPL-2/p105 and linear ubiquitin octamers (M1-Ub) to a similar degree to GST-ABIN-2 WT (Fig. S2, A and B). Interactions of GST-ABIN-2 to the ESCRT-1 components TSG101 and ALIX (Banks et al., 2016) were also unaffected by *TNIP2*^{E255K} mutation (Fig. S2 C). However, *TNIP2*^{E255K} mutation resulted in a 70% reduction (± 5% SEM) in binding of GST-ABIN-2 to A20 (Fig. 3 B). Together, these results demonstrated that *TNIP2*^{E255K} mutation specifically impaired the interaction of ABIN-2 with A20, without affecting ABIN-2 binding to other known interacting proteins.

ABIN-2–A20 interaction negatively regulates HDM airway allergic responses

To investigate the role of ABIN-2–A20 interaction in HDM allergic responses, we generated the *Tnip2*$^{E256K/E256K}$ knock-in mouse strain expressing ABIN-2^{E256K}, the mouse equivalent of the human ABIN-2^{E255K} variant (Fig. S2 D). *Tnip2*$^{E256K/E256K}$ mice were produced in expected Mendelian ratios and were of normal

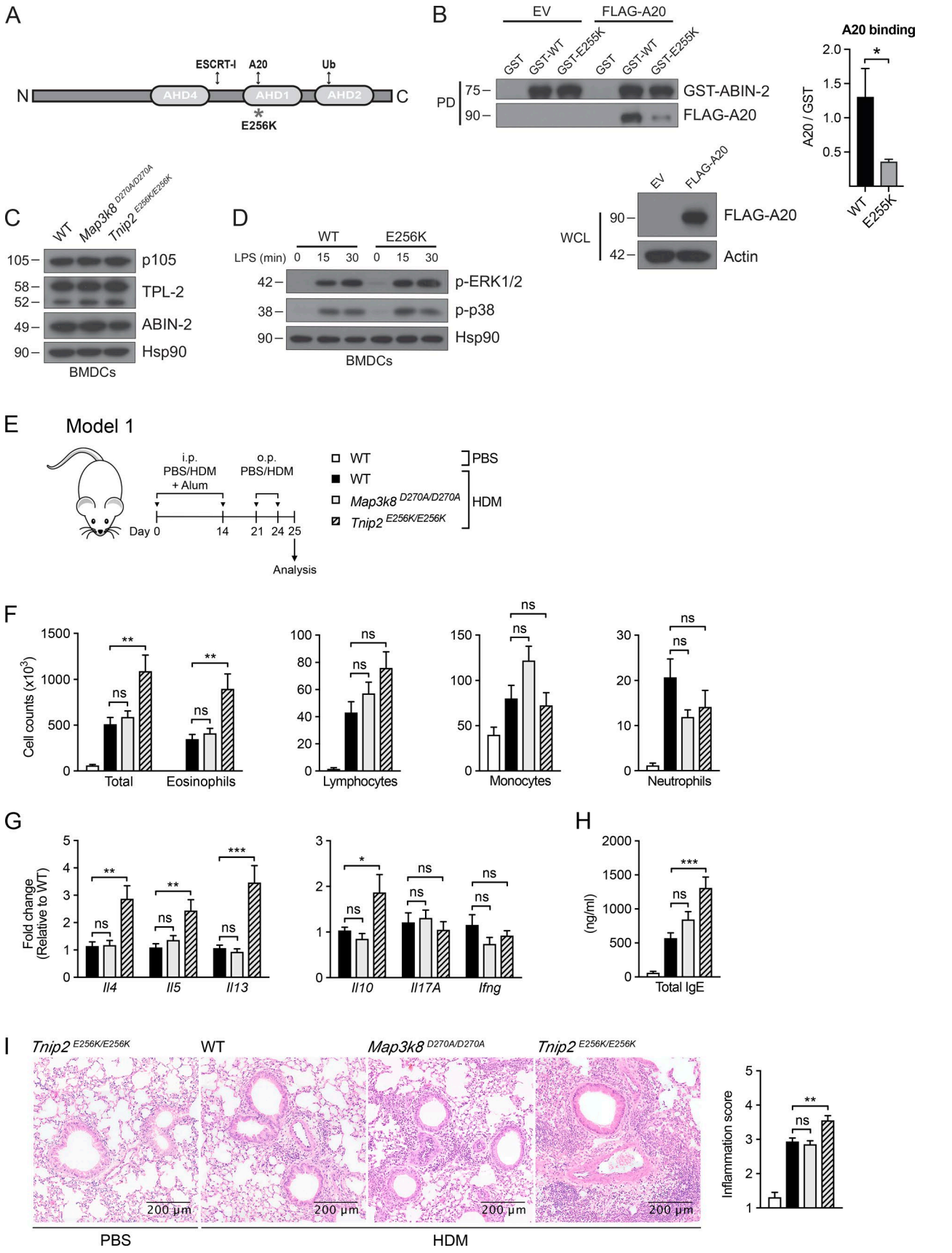

Figure 3. **ABIN-2–A20 interaction negatively regulates HDM-induced allergic responses. (A)** Schematic representation of ABIN-2 domains and protein interactions. **(B)** FLAG-A20 was transiently expressed in HEK293 cells. Interaction with GST-ABIN-2 and GST-ABIN-2^{E256K} was determined in pulldown assays (left). A20 binding was quantified from three independent experiments. Unpaired two-tailed *t* test. EV, empty vector; WCL, whole cell lysate. **(C)** Lysates of

weight, with no obvious phenotype. Full necropsy of 8-mo-old *Tnip2*$^{E256K/E256K}$ mice revealed no signs of inflammation in any tissue (data not shown). TPL-2 protein levels in *Tnip2*$^{E256K/E256K}$ BMDCs were similar to WT cells (Fig. 3 C), and TPL-2–dependent activation of ERK-1/2 following LPS stimulation of BMDCs (Kaiser et al., 2009) was unaffected by *Tnip2*^{E256K} mutation (Fig. 3 D). *Tnip2*^{E256K} mutation therefore allowed the function of ABIN-2–A20 interaction in allergy to be investigated without any confounding effects on TPL-2 signaling.

Compared with WT controls, *Tnip2*$^{E256K/E256K}$ mice developed exacerbated airway inflammation following HDM/Alum sensitization and oropharyngeal HDM challenge (Model 1). This was characterized by significantly increased eosinophilia (Fig. 3 F), lung mRNA expression of Th2 cytokines (*Il4*, *Il5*, and *Il13*) and *Il10* (Fig. 3 G), and serum IgE (Fig. 3 H), with more pronounced peribronchovascular infiltrates (Fig. 3 I). The HDM allergic response of *Map3k8*$^{D270A/D270A}$ mice challenged in parallel was equivalent to WT controls, as expected. Similarly, adoptive transfer of HDM-pulsed *Tnip2*$^{E256K/E256K}$ BMDCs into C57BL/6 recipients (Model 2) augmented pulmonary inflammation compared with WT BMDC transfer following HDM challenge, in all parameters tested, in contrast to adoptive transfer with HDM-pulsed *Map3k8*$^{D270A/D270A}$ BMDCs (Fig. S3).

Tnip2$^{E256K/E256K}$ mice were also tested in a new acute model of allergic asthma (Haspeslagh et al., 2017), in which HDM sensitization was performed via the oropharyngeal route followed by intranasal challenges, removing the requirement for adjuvant (Model 3; Fig. 4 A). Similar to the HDM/Alum model, *Tnip2*^{E256K} mutation exacerbated the allergic response to HDM (Fig. 4). BAL eosinophil numbers (Fig. 4 B), Th2 cytokine (*Il4*, *Il5*, and *Il13*), *Il10* and *Il17A* mRNA expression in the lung (Fig. 4 C), serum IgE (Fig. 4 D), and pulmonary inflammation (Fig. 4 E) were significantly elevated in *Tnip2*$^{E256K/E256K}$ mice compared with WT controls after HDM challenge. *Map3k8*^{D270A} mutation did not significantly alter the allergic response to HDM (Fig. 4, B–E), consistent with results using HDM allergy Models 1 and 2.

Reduction of ABIN-2–A20 interaction by *Tnip2*^{E256K} mutation, therefore, increased the acute airway allergic response to HDM independently of the route of antigen administration and of any adjuvant-associated effects. This is consistent with the hypothesis that the augmented HDM allergic response of *Map3k8*$^{-/-}$mice results from a reduction in ABIN-2–A20 complex formation caused by ABIN-2 deficiency.

Homozygous deletion of *Tnfaip3* in DC in *Tnfaip3*$^{fl/fl}$ *CD11c-Cre* mice blocks eosinophilic inflammation in the acute oropharyngeal HDM allergy model (Model 3), while inducing strong neutrophilic inflammation (Vroman et al., 2018). In contrast, *Tnip2*^{E256K} mutation promoted both eosinophilic and neutrophilic inflammation in this model, similar to *Tnfaip3*$^{fl/+}$ *CD11c-Cre* mice which express reduced levels of A20 in DCs (Vroman et al., 2018). A20 deficiency stimulates neutrophilic inflammation by inducing Th17 differentiation and IL-17A production in the lungs. Consistent with this, *Tnip2*^{E256K} mutation in intact mice increased lung *Il17a* mRNA levels after oropharyngeal HDM sensitization and challenge (Model 3). *Tnip2*^{E256K} mutation also induced neutrophil inflammation in the BMDC transfer model of HDM-induced asthma (Model 2), which again correlated with increased lung *Il17a* mRNA expression, in addition to inducing eosinophilia. In contrast, *Tnip2*^{E256K} mutation promoted eosinophil lung infiltration using the HDM/Alum asthma protocol (Model 1) and did not increase *Il17a* mRNA expression or induce neutrophilia in the lungs. ABIN-2, therefore, was able to suppress HDM allergic responses independently of effects on IL-17A expression and neutrophil inflammation in this model.

CCL24 overproduction by lung DCs exacerbates HDM-induced allergic inflammation in *Tnip2*$^{E256K/E256K}$ mice

We have previously shown that the increased airway allergic inflammation in *Map3k8*$^{-/-}$ mice following HDM challenge results from overproduction of CCL24 by lung DCs (Kannan et al., 2016). To determine whether the inflammatory effects of *Tnip2*^{E256K} mutation also involved CCL24 production by DCs, we first sorted lung CD11c^{+} MHC-II^{+} DCs from local draining mediastinal lymph nodes of *Tnip2*$^{E256K/E256K}$ and WT mice after oropharyngeal HDM sensitization. Quantitative RT-PCR (qRT-PCR) demonstrated that *Tnip2*^{E256K} mutation resulted in a significant increase in *Ccl24* mRNA expression in lung DC, while *Map3k8*^{D270A} mutation had no effect (Fig. 5 A). Consistent with CCL24 overproduction exacerbating HDM-induced allergic inflammation, *Ccl24* mRNA in lungs and CCL24 protein in BAL fluid was increased in all three models of HDM-induced airway inflammation (Fig. 5 B). In contrast, *Map3k8*^{D270A} mutation did not affect *Ccl24* lung mRNA expression or CCL24 protein levels in BAL fluid following HDM challenge in each of these models (Fig. 5 B).

We next investigated whether CCL24 induced in DCs by *Tnip2*^{E256K} mutation caused the exacerbation in HDM-induced allergic airway inflammation (Model 4; Fig. 5 A). Naive WT mice were inoculated with HDM-pulsed WT or *Tnip2*$^{E256K/E256K}$ BMDCs and challenged three times with HDM plus CCL24 neutralizing antibody or isotype control IgG (Kannan et al., 2016). CCL24 blockade had minimal effect on airway inflammation in mice given WT BMDCs, but prevented the severe airway inflammation that developed in mice with adoptively transferred *Tnip2*$^{E256K/E256K}$ BMDCs. Anti-CCL24 significantly reduced eosinophilia (Fig. 5 D), lung *Il4*, *Il5*, and *Il10* mRNA expression (Fig. 5 E), serum IgE (Fig. 5 F), and pulmonary inflammation (Fig. 5 G) promoted by

BMDCs generated from the indicated genotypes were probed for ABIN-2, TPL-2, and NF-κB1 p105. Data are representative of three independent experiments. **(D)** Lysates from LPS-stimulated BMDCs were immunoblotted for the indicated antigens. Data are representative of two independent experiments. **(E)** Schematic representation of HDM/Alum-dependent allergy model (Model 1). o.p., oropharyngeal. **(F)** Differential cell counts in BAL fluids of PBS and HDM-challenged WT, *Map3k8*$^{D270A/D270A}$, and *Tnip2*$^{E256K/E256K}$ mice. **(G)** Cytokines mRNA expression levels in the lung, as assessed by qRT-PCR. **(H)** Total IgE levels in blood serum, as assessed by ELISA. **(I)** H&E-stained lung sections (left) and inflammation scores (right) from PBS and HDM-challenged mice. Data in panels F–I are shown as mean ± SEM and are pooled from three independent experiments (n = 10–15 mice/genotype). *, $P < 0.05$; **, $P < 0.005$; ***, $P < 0.001$. Comparisons assessed by Kruskal-Wallis and Dunn-Bonferroni's post hoc test. ns, not significant.

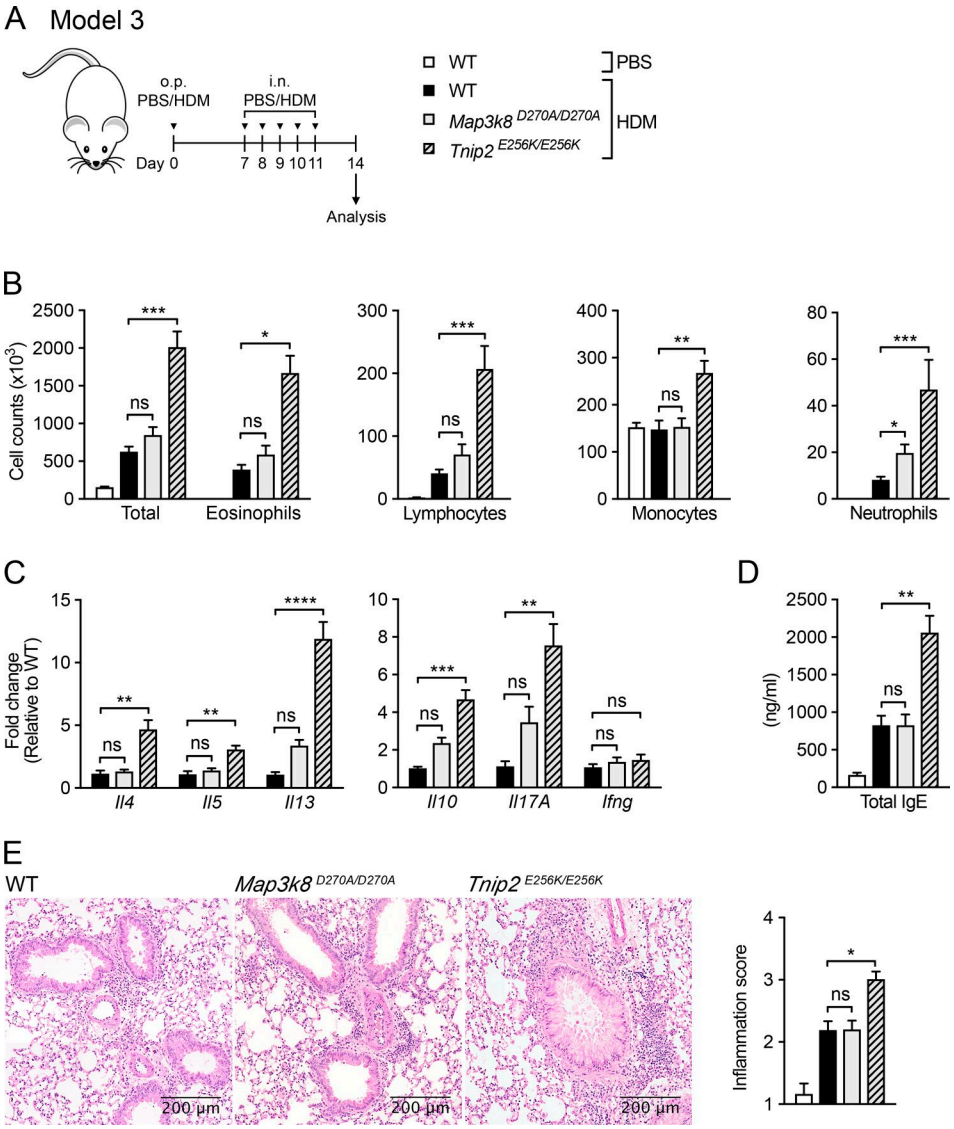

Figure 4. ***Tnip2*$^{E256K/E256K}$ mice developed exacerbated airway inflammation in an acute model of allergic asthma. (A)** Schematic representation of Alum-independent, intranasal HDM-induced allergy model (Model 3). o.p., oropharyngeal. Samples were collected for analysis 3 d after the last HDM challenge. **(B)** Differential cell counts in BAL fluids of PBS- and HDM-challenged WT, *Map3k8*$^{D270A/D270A}$, and *Tnip2*$^{E256K/E256K}$ mice. **(C)** Cytokines mRNA expression levels in the lung, as assessed by qRT-PCR. **(D)** Total IgE levels in blood serum, as assessed by ELISA. **(E)** H&E-stained lung sections (left) and inflammation scores (right) from PBS- and HDM-challenged mice. Data in panels B–E are shown as mean ± SEM and are pooled from three independent experiments (n = 13–15 mice/genotype). *, P < 0.05; **, P < 0.005; ***, P < 0.001; ****, P < 0.0001. Comparisons assessed by Kruskal-Wallis and Dunn-Bonferroni's post hoc test. ns, not significant.

adoptive transfer of *Tnip2*$^{E256K/E256K}$ BMDCs. Collectively, these data suggest that ABIN-2–A20 interaction in DCs prevents acute severe airway allergic responses to HDM by suppressing DC production of CCL24.

Concluding comments

We have previously shown that *Map3k8*$^{-/-}$ mice develop more pronounced type 2 airway inflammation to HDM sensitization and challenge compared with WT controls (Kannan et al., 2016). Using *Map3k8*$^{D270A/D270A}$ mice, we show here that TPL-2 kinase activity did not regulate HDM-induced airway inflammation, revealing an unappreciated adaptor function for TPL-2 in inflammation. TPL-2 is required to stabilize ABIN-2 protein (Sriskantharajah et al., 2014), and we demonstrate that *Tnip2*^{E256K} mutation phenocopied the effect of TPL-2 deficiency in HDM-induced allergic airway inflammation. These results suggest that the augmented HDM-induced allergic response of *Map3k8*$^{-/-}$ mice is caused by reduced ABIN-2 levels, which impairs ABIN2 complex formation with the key negative regulator of inflammation A20 (Dong et al., 2011; Catrysse et al., 2014). Our results also imply that TPL-2 inhibition would not have adverse effects on allergic responses. This is an important consideration for the continued development of TPL-2 inhibitors to treat inflammatory diseases and cancer.

DC-specific deletion of *Tnfaip3* increases DC numbers by blocking apoptosis and induces constitutive expression of DC activation markers. This results in systemic inflammation that resembles lupus erythematosus (Kool et al., 2011). *Tnip2*^{E256K} mutation mim-

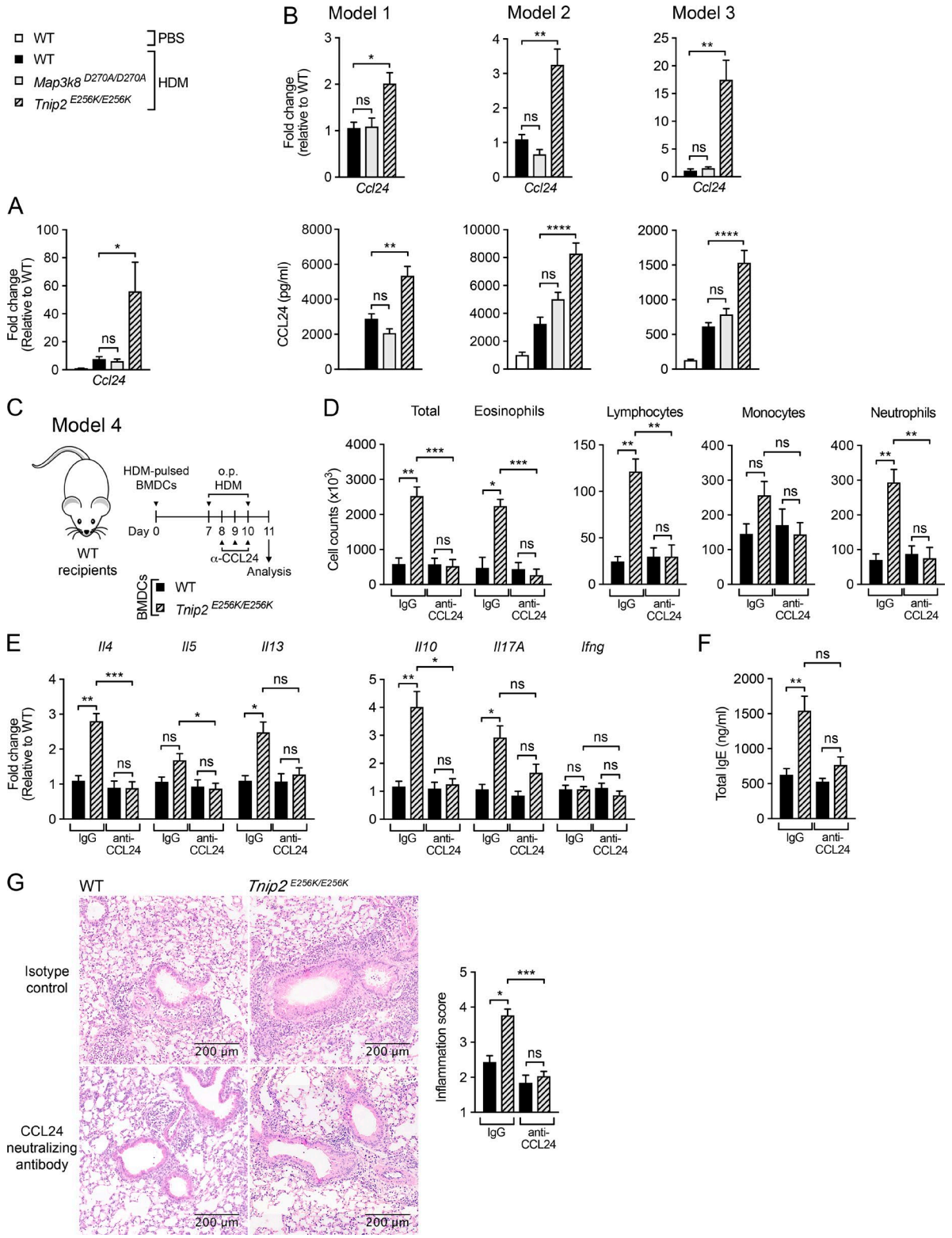

Figure 5. **CCL24 neutralization rescues the exaggerated allergic response to HDM in *Tnip2*$^{E256K/E256K}$ BMDC adoptively transferred mice. (A)** *Ccl24* mRNA levels in sorted CD11c^{+} MHC-II^{+} DCs from lung draining mediastinal lymph nodes, collected 3 d after oropharyngeal HDM sensitization, were determined by qRT-PCR. **(B)** CCL24 protein levels in the BAL fluid (bottom panels) and mRNA levels in the lung (top panels) for all three HDM-induced allergy models. **(C)** Schematic representation of CCL24 neutralization experimental setup, in the HDM-pulsed BMDCs adoptive transfer model (Model 4). o.p., oropharyngeal. **(D)** Differential cell counts in BAL fluids of HDM-challenged WT mice given either isotype control or anti-CCL24 neutralizing antibody, after adoptive transfer of HDM-pulsed WT or *Tnip2*$^{E256K/E256K}$ BMDCs. **(E)** mRNA expression levels in the lung, as assessed by qRT-PCR. **(F)** Total IgE levels in blood serum, as assessed by ELISA. **(G)** H&E-stained lung sections (left) and inflammation scores (right). Data in panels A, B, and D–G are shown as mean ± SEM and are pooled from two independent experiments (n = 8–9 mice/genotype). *, P < 0.05; **, P < 0.005; ***, P < 0.001; ****, P < 0.0001. Indicated comparisons were assessed by Kruskal-Wallis and Dunn-Bonferroni's post hoc test. ns, not significant.

icked some of the effects of reduced A20 expression in DCs in acute HDM-induced airway inflammation (Vroman et al., 2018). However, *Tnip2*^{E256K} mutation did not affect DC homeostasis, induce spontaneous DC activation, or promote systemic inflammation (data not shown). The more restricted impact of *Tnip2*^{E256K} mutation on DC function may be due in part to the fractional reduction, but not absence, of ABIN-2–A20 interaction. Alternatively, ABIN-2 may only be important in mediating some of the downstream functions of A20, which are mediated via multiple effectors, such as NLRP3, RIPK1, and MALT1 (Das et al., 2018). This may explain why *Tnip2* has not been identified in GWAS for asthma and allergy, in contrast to *Tnfaip3* (Li et al., 2012; Schuijs et al., 2015).

Materials and methods

Animals

All mice were bred and maintained under specific pathogen–free conditions at the Francis Crick Institute, and all experiments were performed in accordance with UK Home Office regulations. Animal work was endorsed by the Francis Crick Institute Animal Welfare and Ethical Review Body. Mouse strains used: WT, *Map3k8*$^{-/-}$ (Dumitru et al., 2000), *Map3k8*$^{D270A/D270A}$ (Sriskantharajah et al., 2014), *Tnip2*$^{-/-}$ (Papoutsopoulou et al., 2006), and *Tnip2*$^{E256K/E256K}$ (this study) were all on a C57BL/6J background.

Antibodies and recombinant proteins

Antibodies were obtained from commercial suppliers or made in house, as indicated: TPL-2 (Santa Cruz; sc-720), ABIN-2 (Lang et al., 2004), GST (Sigma; A7340), Hsp90 (Santa Cruz; sc-7947), HA (Roche; 11867423001), p-ERK1/2 (Cell Signaling; 9101), 3×FLAG (Sigma; F1804), M1 Ubiquitin (Merck; MABS451), p-p38 (Cell Signaling; 4511), ABIN-1 (MRC Protein Phosphorylation & Ubiquitylation Unit, University of Dundee, Dundee, Scotland, UK), tubulin (a gift from K. Gull; University of Oxford); NF-κB1 p105 (Cell Signaling; 4717), Actin (Santa Cruz; sc-1615), and His_6 (Sigma; A7058).

cDNAs encoding human ABIN-2 WT and ABIN-2^{E255K} proteins were sub-cloned in pGex-6P-1 expression vector (Invitrogen) by the MRC Protein Phosphorylation & Ubiquitylation Unit (University of Dundee). Recombinant proteins were expressed in *Escherichia coli* and purified on glutathione Sepharose 4B resin, using standard methods.

HDM/Alum model of Th2 airway allergic inflammation (Model 1)

Female mice (8–12 wk old) were sensitized on days 0 and 14 via the intraperitoneal route with PBS (vehicle) or 100 µg (dry weight) of HDM (*Dermatophagoides pternoyssinus* extracts; Greer), in the presence of Imject Alum (in PBS solution [1:3]; Thermo Scientific). Following sensitization, mice were challenged twice (on days 21 and 24) via the oropharyngeal route with 100 µg of HDM, diluted in PBS or vehicle (PBS). All the parameters for airway allergy were measured 1 d after the last challenge.

Adoptive transfer model of HDM-induced airway allergic inflammation (Model 2)

Bone marrow cells from female mice (8–10 wk old) were cultured in the presence of 20 ng/ml GM-CSF (Peprotech) for 10 d (Kaiser et al., 2009). BMDCs were pulsed overnight with 10 µg of HDM or PBS (vehicle), in media containing 5 ng/ml GM-CSF. Cells were then washed with PBS and transferred oropharyngeally into naive WT recipient mice (Lambrecht et al., 2000). Following BMDC transfer, recipient mice were challenged via the oropharyngeal route with 100 µg of HDM, diluted in PBS or PBS vehicle on days 7 and 10. Airway allergy parameters were analyzed on day 11.

Alum-independent oropharyngeal HDM sensitization model of HDM-induced airway allergic inflammation (Model 3)

Female mice (8–12 wk old) were sensitized on day 0 via the oropharyngeal route with 100 µg of HDM in PBS or vehicle (PBS) and subsequently challenged intranasally with 10 µg of HDM over a period of 5 d from day 7 to day 11. All the parameters for airway allergy were measured 3 and 7 d after the last challenge.

CCL24 neutralization in the adoptive transfer model of HDM-induced airway allergic inflammation (Model 4)

Neutralizing CCL24 antibodies diluted in PBS (Mouse CCL24/eotaxin-2 Monoclonal Rat IgG_{2A} [Clone 106521; R&D Systems-Biotechne; MAB528], and Mouse CCL24/eotaxin-2 Affinity Purified Polyclonal Goat IgG [R&D Systems-Biotechne; AF528]) were mixed and used at 0.03 mg/dose (monoclonal) and 0.006 mg/dose (polyclonal). Isotype controls Monoclonal Rat IgG_{2A} (Clone 54447; R&D Systems-Biotechne; MAB006) and Normal Goat IgG (R&D Systems-Biotechne; AB-108-C) were mixed and used in similar ratios. Antibody mixes were administered via the intraperitoneal route on days 8, 9, and 10 of the adoptive transfer model of HDM allergy (Model 2).

Phenotypic characterization of HDM-induced airway inflammation

Serum, BAL fluid, and lung tissue were collected for each mouse. BAL fluid was collected in 1.2 ml of PBS and centrifuged at 2,000 *g* for 10 min at 4°C. Cells were resuspended in 200 µl PBS and total cell numbers were counted; BAL fluid was stored at −80°C for further analysis. Differential cell counts were performed on Giemsa-stained cytospins (Sigma).

ELISAs and immunoblotting

IL-5, IL-13, CCL24, and total IgE levels were measured using DuoSet ELISA kits, according to the manufacturer's instructions (R&D Systems-Biotechne).

Cell lysates (normalized to equal total protein content) or GST pulldowns were resolved on 10% Tris-Glycine gels. Separated proteins were transferred onto polyvinylidene difluoride membranes using the Trans-Blot Turbo Transfer System (Bio-Rad). Specific bound antibodies were visualized by chemiluminescence (Immobilon, Merck Millipore; ECL, GE Healthcare).

Lung histopathology

Excised lungs were fixed in 10% neutral buffered formalin overnight and washed in 75% ethanol. Tissues were embedded in paraffin and lung sections were stained with H&E. Stained slides were scanned with Axio-Scan.Z1 slide scanner (Zeiss) and im-

ages were analyzed using ZEN Lite software. A semi-quantitative scoring system was used to grade the size of lung infiltrates, as described (Lloyd et al., 2001). In brief, a score of 5 signified a large (less than three cells deep) widespread inflammatory infiltrate around the majority of vessels and bronchioles, and a score of 1 represented a small (less than or equal to two cells deep) number of inflammatory foci.

GST pulldowns

HA-tagged NF-κB1 p105 (HA-p105; Salmerón et al., 2001), His_6-tagged TPL-2 (His_6-TPL-2), 3×FLAG-tagged A20 (3×FLAG-A20; from MRC Protein Phosphorylation Unit, University of Dundee), ALIX (3×FLAG-ALIX), and TSG101 (3×FLAG-TSG101) cDNA were separately sub-cloned into the pcDNA3 vector (Invitrogen). All constructs were confirmed by DNA sequencing. Recombinant proteins were transiently overexpressed in adherent HEK293 cells by transfection with a polyethylenimine (Sigma)/plasmid vector mixture in a 3:1 ratio (wt/wt). After 24 h culture, HEK293 cells were lysed in buffer A (50 mM Tris, pH 7.5, 150 mM NaCl, 1% Triton X-100, 10 mM sodium fluoride, 1 mM sodium pyrophosphate, 10 mM β-glycerophosphate, 2 mM EDTA, 0.1 mM sodium orthovanadate, 10% glycerol, and EDTA-free protease inhibitor cocktail; Roche). 750 µg of HEK293 cell lysate, cleared by centrifugation, was incubated with 2 µg purified GST protein or 2.9 µg purified GST-ABIN-2 fusion protein and glutathione Sepharose 4B resin (10 µl packed beads; GE Healthcare). After overnight incubation at 4°C with mixing, beads were washed six times with buffer A and boiled in SDS-PAGE sample buffer for 10 min at 95°C.

For ubiquitin pulldowns, 2 µg purified GST protein or 2.9 µg purified GST-ABIN-2 fusion protein was incubated with glutathione Sepharose 4B resin (GE Healthcare) and 500 ng/ml purified M1 poly-ubiquitin (2,4,8) mixture (Enzo Life Sciences) in binding buffer (50 mM Tris, pH 7.5, 150 mM NaCl, 5 mM DTT, and 0.1% NP-40) for 3 h at 4°C. Beads were washed five times with binding buffer and boiled in SDS-PAGE sample buffer for 10 min at 95°C.

Statistical analysis

Data were analyzed using Prism 7 (GraphPad Software). Statistical analysis was performed using the nonparametric Kruskal-Wallis test ($\alpha = 0.05$) followed by Dunn's multiple comparison test and Bonferroni correction. Data shown represent means ± SEM, and are pooled from at least three independent experiments. Adjusted P values of <0.05 (*), <0.005 (**), <0.001 (***), and <0.0001 (****) were considered significant.

Online supplemental material

Fig. S1 shows protein levels of TPL-2 and ABIN-2 in BMDCs generated from *Map3k8*$^{-/-}$ and *Tnip2*$^{-/-}$ mice and respective phenotype in HDM-induced allergy models 1 and 2 compared with WT mice. Fig. S2 shows the effect of the TNIP2^{E255K} mutation in binding of ABIN-2 to known interactors (M1-Ub chains, TPL-2, p105, ALIX, and TSG101) and the schematic representation of the targeting vector used to create *Tnip2*$^{E256K/E256K}$ mice. Fig. S3 shows the phenotype of WT, *Map3k8*$^{D270A/D270A}$ and *Tnip2*$^{E256K/E256K}$ BMDCs adoptively transferred mice (Model 2).

Acknowledgments

We are grateful to the Francis Crick Institute Flow Cytometry, Biological Research, and Histopathology Facilities for their help during the production of this work. We also thank members of the Ley Laboratory, Professor Clare Lloyd (Imperial College London, London, England, UK), and Professor Caetano Reis e Sousa (Francis Crick Institute) for their advice and support during this project.

This work was supported by the Francis Crick Institute (FC001103), which is funded by the Medical Research Council, Cancer Research UK, and the Wellcome Trust and a Bloodwise Project Grant (12040). F. Breyer was funded on a Boehringer Ingelheim Fonds PhD fellowship.

The authors declare no competing financial interests.

Author contributions: S. Ventura and F. Cano performed the majority of in vivo of experiments. Y. Kannan performed the initial in vivo experiments with *Tnip2*$^{E256K/E256K}$ mice. F. Breyer performed the biochemical analyses. M.J. Pattison assisted with some of the in vivo experiments. M.S. Wilson provided advice for the project and edited the manuscript. S. Ventura, F. Cano, and S.C. Ley planned the experiments and wrote the manuscript.

Submitted: 24 May 2017
Revised: 20 August 2018
Accepted: 5 October 2018

References

Banks, C.A.S., G. Boanca, Z.T. Lee, C.G. Eubanks, G.L. Hattem, A. Peak, L.E. Weems, J.J. Conkright, L. Florens, and M.P. Washburn. 2016. TNIP2 is a hub protein in the NF-kappaB network with both protein and RNA mediated interactions. *Mol. Cell. Proteomics.* 15:3435–3449. https://doi.org/10.1074/mcp.M116.060509

Catrysse, L., L. Vereecke, R. Beyaert, and G. van Loo. 2014. A20 in inflammation and autoimmunity. *Trends Immunol.* 35:22–31. https://doi.org/10.1016/j.it.2013.10.005

Das, T., Z. Chen, R.W. Hendriks, and M. Kool. 2018. A20/Tumor Necrosis Factor alpha-induced Protein 3 in immune cells controls development of autoinflammation and autoimmunity: lessons from mouse models. *Front. Immunol.* 9:104. https://doi.org/10.3389/fimmu.2018.00104

Dong, G., E. Chanudet, N. Zeng, A. Appert, Y.-W. Chen, W.-Y. Au, R.A. Hamoudi, A.J. Watkins, H. Ye, H. Liu, et al. 2011. A20, ABIN-1/2, and CARD11 mutations and their prognostic value in gastrointestinal diffuse large B-cell lymphoma. *Clin. Cancer Res.* 17:1440–1451. https://doi.org/10.1158/1078-0432.CCR-10-1859

Dumitru, C.D., J.D. Ceci, C. Tsatsanis, D. Kontoyiannis, K. Stamatakis, J.-H. Lin, C. Patriotis, N.A. Jenkins, N.G. Copeland, G. Kollias, and P.N. Tsichlis. 2000. TNF-alpha induction by LPS is regulated posttranscriptionally via a Tpl2/ERK-dependent pathway. *Cell.* 103:1071–1083. https://doi.org/10.1016/S0092-8674(00)00210-5

Gantke, T., S. Sriskantharajah, and S.C. Ley. 2011. Regulation and function of TPL-2, an IκB kinase-regulated MAP kinase. *Cell Res.* 21:131–145. https://doi.org/10.1038/cr.2010.173

Gantke, T., S. Sriskantharajah, M. Sadowski, and S.C. Ley. 2012. IκB kinase regulation of the TPL-2/ERK MAPK pathway. *Immunol. Rev.* 246:168–182. https://doi.org/10.1111/j.1600-065X.2012.01104.x

George, D., and A. Salmeron. 2009. Cot/Tpl-2 protein kinase as a target for the treatment of inflammatory disease. *Curr. Top. Med. Chem.* 9:611–622. https://doi.org/10.2174/156802609789007345

Gutmann, S., A. Hinniger, G. Fendrich, P. Drückes, S. Antz, H. Mattes, H. Möbitz, S. Ofner, N. Schmiedeberg, A. Stojanovic, et al. 2015. The crystal structure of Cancer Osaka Thyroid kinase reveals an unexpected kinase domain fold. *J. Biol. Chem.* 290:15210–15218. https://doi.org/10.1074/jbc.M115.648097

Haspeslagh, E., N. Debeuf, H. Hammad, and B.N. Lambrecht. 2017. Murine models of allergic asthma. *Methods Mol. Biol.* 1559:121–136. https://doi.org/10.1007/978-1-4939-6786-5_10

Kaiser, F., D. Cook, S. Papoutsopoulou, R. Rajsbaum, X. Wu, H.T. Yang, S. Grant, P. Ricciardi-Castagnoli, P.N. Tsichlis, S.C. Ley, and A. O'Garra. 2009. TPL-2 negatively regulates interferon-beta production in macrophages and myeloid dendritic cells. *J. Exp. Med.* 206:1863–1871. https://doi.org/10.1084/jem.20091059

Kannan, Y., Y. Li, S.M. Coomes, I.S. Okoye, V.S. Pelly, S. Sriskantharajah, E. Gückel, L. Webb, S. Czieso, N. Nikolov, et al. 2016. TPL-2 reduces severe allergic airway inflammation by inhibiting Ccl24 production in dendritic cells. *J. Allergy Clin. Immunol.* 139:655–666. https://doi.org/10.1016/j.jaci.2016.05.031

Kool, M., G. van Loo, W. Waelput, S. De Prijck, F. Muskens, M. Sze, J. van Praet, F. Branco-Madeira, S. Janssens, B. Reizis, et al. 2011. The ubiquitin-editing protein A20 prevents dendritic cell activation, recognition of apoptotic cells, and systemic autoimmunity. *Immunity.* 35:82–96. https://doi.org/10.1016/j.immuni.2011.05.013

Lambrecht, B.N., M. De Veerman, A.J. Coyle, J.C. Gutierrez-Ramos, K. Thielemans, and R.A. Pauwels. 2000. Myeloid dendritic cells induce Th2 responses to inhaled antigen, leading to eosinophilic airway inflammation. *J. Clin. Invest.* 106:551–559. https://doi.org/10.1172/JCI8107

Lang, V., A. Symons, S.J. Watton, J. Janzen, Y. Soneji, S. Beinke, S. Howell, and S.C. Ley. 2004. ABIN-2 forms a ternary complex with TPL-2 and NF-kappa B1 p105 and is essential for TPL-2 protein stability. *Mol. Cell. Biol.* 24:5235–5248. https://doi.org/10.1128/MCB.24.12.5235-5248.2004

Li, X., E.J. Ampleford, T.D. Howard, W.C. Moore, D.G. Torgerson, H. Li, W.W. Busse, M. Castro, S.C. Erzurum, E. Israel, et al. 2012. Genome-wide association studies of asthma indicate opposite immunopathogenesis direction from autoimmune diseases. *J. Allergy Clin. Immunol.* 130:861–8.e7. https://doi.org/10.1016/j.jaci.2012.04.041

Lloyd, C.M., J.-A. Gonzalo, T. Nguyen, T. Delaney, J. Tian, H. Oettgen, A.J. Coyle, and J.C. Gutierrez-Ramos. 2001. Resolution of bronchial hyperresponsiveness and pulmonary inflammation is associated with IL-3 and tissue leukocyte apoptosis. *J. Immunol.* 166:2033–2040. https://doi.org/10.4049/jimmunol.166.3.2033

Papoutsopoulou, S., A. Symons, T. Tharmalingham, M.P. Belich, F. Kaiser, D. Kioussis, A. O'Garra, V. Tybulewicz, and S.C. Ley. 2006. ABIN-2 is required for optimal activation of Erk MAP kinase in innate immune responses. *Nat. Immunol.* 7:606–615. https://doi.org/10.1038/ni1334

Pattison, M.J., O. Mitchell, H.R. Flynn, C.-S. Chen, H.-T. Yang, H. Ben-Addi, S. Boeing, A.P. Snijders, and S.C. Ley. 2016. TLR and TNF-R1 activation of the MKK3/MKK6-p38α axis in macrophages is mediated by TPL-2 kinase. *Biochem. J.* 473:2845–2861. https://doi.org/10.1042/BCJ20160502

Salmerón, A., J. Janzen, Y. Soneji, N. Bump, J. Kamens, H. Allen, and S.C. Ley. 2001. Direct phosphorylation of NF-kappaB1 p105 by the IkappaB kinase complex on serine 927 is essential for signal-induced p105 proteolysis. *J. Biol. Chem.* 276:22215–22222. https://doi.org/10.1074/jbc.M101754200

Schuijs, M.J., M.A. Willart, K. Vergote, D. Gras, K. Deswarte, M.J. Ege, F.B. Madeira, R. Beyaert, G. van Loo, F. Bracher, et al. 2015. Farm dust and endotoxin protect against allergy through A20 induction in lung epithelial cells. *Science.* 349:1106–1110. https://doi.org/10.1126/science.aac6623

Sriskantharajah, S., E. Gückel, N. Tsakiri, K. Kierdorf, C. Brender, A. Ben-Addi, M. Veldhoen, P.N. Tsichlis, B. Stockinger, A. O'Garra, et al. 2014. Regulation of experimental autoimmune encephalomyelitis by TPL-2 kinase. *J. Immunol.* 192:3518–3529. https://doi.org/10.4049/jimmunol.1300172

Van Huffel, S., F. Delaei, K. Heyninck, D. De Valck, and R. Beyaert. 2001. Identification of a novel A20-binding inhibitor of nuclear factor-kappa B activation termed ABIN-2. *J. Biol. Chem.* 276:30216–30223. https://doi.org/10.1074/jbc.M100048200

Vroman, H., I.M. Bergen, J.A.C. van Hulst, M. van Nimwegen, D. van Uden, M.J. Schuijs, S.Y. Pillai, G. van Loo, H. Hammad, B.N. Lambrecht, et al. 2018. TNF-α-induced protein 3 levels in lung dendritic cells instruct T_H2 or T_H17 cell differentiation in eosinophilic or neutrophilic asthma. *J. Allergy Clin. Immunol.* 141:1620–1633.e12. https://doi.org/10.1016/j.jaci.2017.08.012

Wagner, S., I. Carpentier, V. Rogov, M. Kreike, F. Ikeda, F. Löhr, C.-J. Wu, J.D. Ashwell, V. Dötsch, I. Dikic, and R. Beyaert. 2008. Ubiquitin binding mediates the NF-kappaB inhibitory potential of ABIN proteins. *Oncogene.* 27:3739–3745. https://doi.org/10.1038/sj.onc.1211042

Watford, W.T., C.-C. Wang, C. Tsatsanis, L.A. Mielke, A.G. Eliopoulos, C. Daskalakis, N. Charles, S. Odom, J. Rivera, J. O'Shea, and P.N. Tsichlis. 2010. Ablation of tumor progression locus 2 promotes a type 2 Th cell response in Ovalbumin-immunized mice. *J. Immunol.* 184:105–113. https://doi.org/10.4049/jimmunol.0803730

Xiao, Y., J. Jin, M. Chang, M. Nakaya, H. Hu, Q. Zou, X. Zhou, G.C. Brittain, X. Cheng, and S.C. Sun. 2014. TPL2 mediates autoimmune inflammation through activation of the TAK1 axis of IL-17 signaling. *J. Exp. Med.* 211:1689–1702. https://doi.org/10.1084/jem.20132640

Supplemental material

Ventura et al., https://doi.org/10.1084/jem.20170852

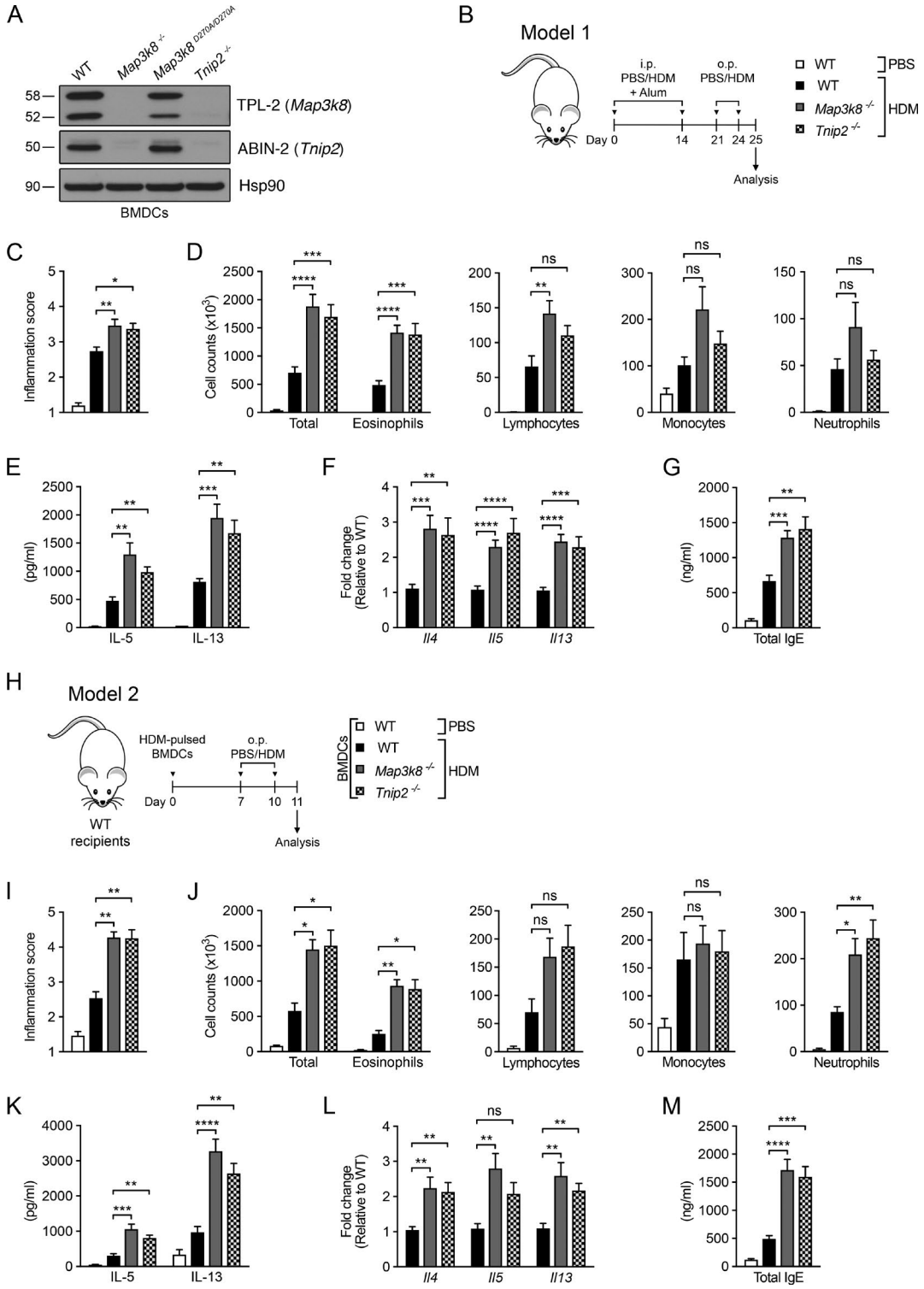

Figure S1. **Deletion of Tnip2 mimics Map3k8$^{-/-}$ phenotype in HDM-induced allergy. (A)** Lysates of BMDCs, generated from the indicated mouse genotypes, were immunoblotted for TPL-2 and ABIN-2. Hsp90 was used as loading control. **(B)** Schematic representation of oropharyngeal HDM sensitization and challenge model in WT, *Map3k8*$^{-/-}$, or *Tnip2*$^{-/-}$ mice. o.p., oropharyngeal. **(C)** Inflammation scores from PBS- and HDM-challenged mice. **(D)** Differential cell counts in BAL fluids of PBS- and HDM-challenged mice. **(E)** Cytokine levels in BAL fluid, as assessed by ELISA. **(F)** Cytokine mRNA expression levels in the lung, measured by qRT-PCR. **(G)** Total IgE levels in blood serum, as assessed by ELISA. **(H)** Schematic representation of BMDC adoptive transfer model of HDM-induced airway allergic inflammation (Model 2). o.p., oropharyngeal. **(I)** Inflammation scores from PBS- or HDM-challenged WT mice after adoptive transfer of HDM-pulsed WT, *Map3k8*$^{-/-}$, or *Tnip2*$^{-/-}$ BMDCs. **(J)** Differential cell counts in BAL fluids of BMDC adoptively transferred mice. **(K)** Cytokine levels in BAL fluid, as assessed by ELISA. **(L)** Cytokines mRNA expression levels in the lung, as assessed by qRT-PCR. **(M)** Total IgE levels in blood serum measured by ELISA. Data in panels C–G and I–M are shown as mean ± SEM and are pooled from three independent experiments (n = 10–15 mice/genotype). *, $P < 0.05$; **, $P < 0.005$; ***, $P < 0.001$; ****, $P < 0.0001$. Comparisons assessed by Kruskal-Wallis and Dunn-Bonferroni's post hoc test. ns, not significant.

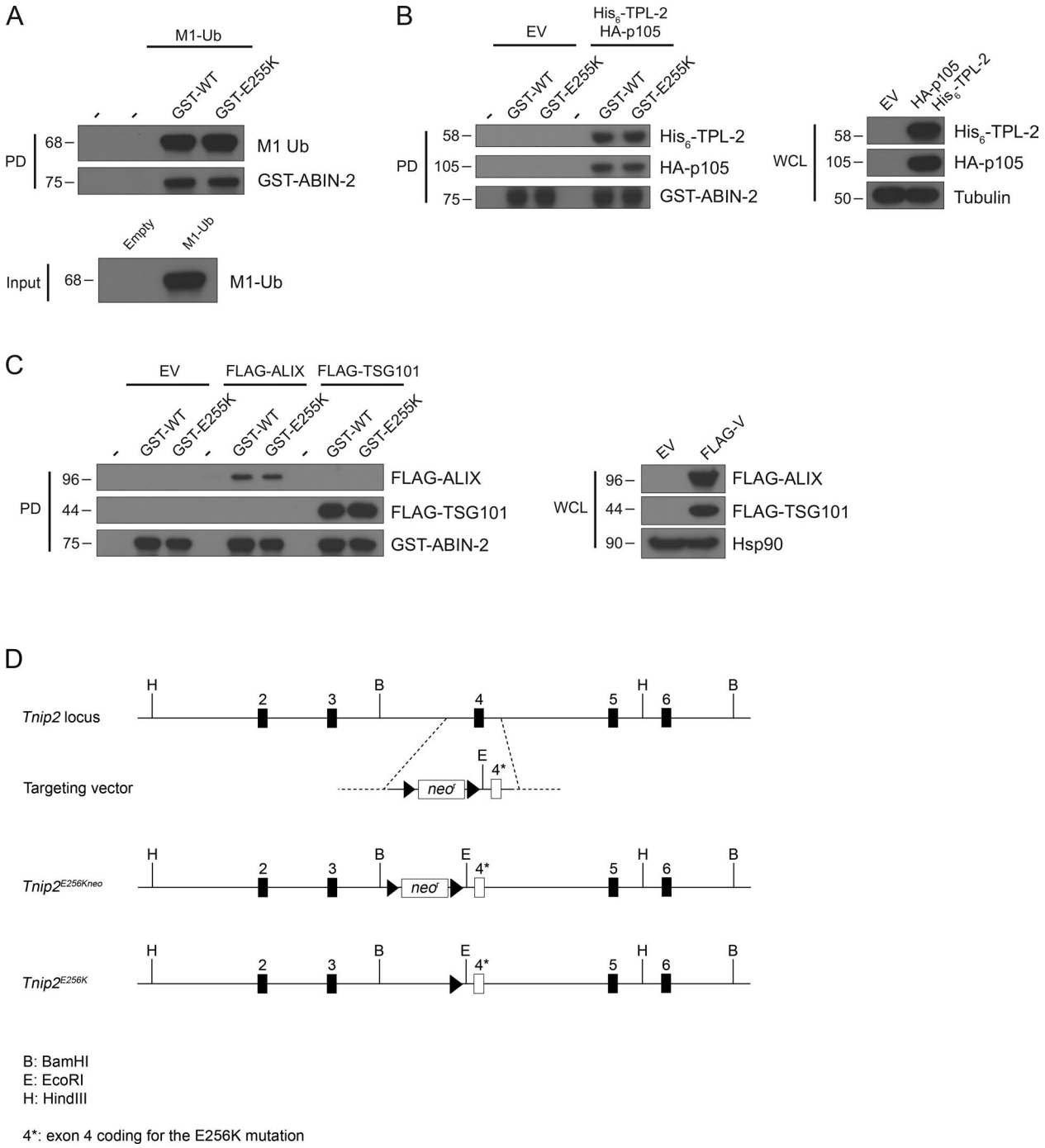

Figure S2. **TNIP2^{E255K} mutation impairs ABIN-2 binding to A20. (A)** Interaction of GST-ABIN-2 and GST-ABIN-2^{E256K} with M1-Ub chains was determined in pulldown assays. Data are representative of three independent experiments. **(B)** His$_6$-TPL-2 and HA-p105 were transiently coexpressed in HEK293 cells. Interaction of GST-ABIN-2 and GST-ABIN-2^{E256K} with His$_6$-TPL-2/HA-p105 complexes was determined in pulldown assays. Data are representative of two independent experiments. **(C)** FLAG-ALIX or FLAG-TSG101 were transiently expressed in HEK293 cells. Interaction of GST-ABIN-2 and GST-ABIN-2^{E256K} with these proteins was determined in pulldown assays. Data are representative of two independent experiments. EV, empty vector; PD, pulldown; WCL, whole cell lysate. **(D)** Schematic representation shows the genomic *Tnip2* locus, the targeting vector, and the mutated *Tnip2^{E256K}* allele. Boxes represent exons. The P381-6.1 *Tnip2^{E256K}*-targeting construct was generated by Gene Bridges GmbH. The FRT-flanked neomycin resistance cassette (PGK-gb2-neo) was inserted in intron 3. Exon 4 encoding E256 was mutated to generate an E256K coding allele, incorporating a new EcoRI restriction site. The final targeting vector was linearized with SalI and electroporated into C57BL/6 ES cells by PolyGene AG. An embryonic stem cell clone (5C4) bearing the E256K mutation was injected into C57BL/6 blastocysts by standard techniques. Male chimeras were bred to C57BL/6J female mice, and progeny was screened by digestion of genomic DNA with HindIII or BamHI, followed by Southern blotting with 5′- and 3′-probes, respectively. This allowed the targeted *Tnip2* alleles to be discriminated from the endogenous *Tnip2* allele. *Tnip2$^{E256K/E256K}$* mice were then crossed with FlpE$^+$ mice for removal of the PGK-gb2-neo sequence.

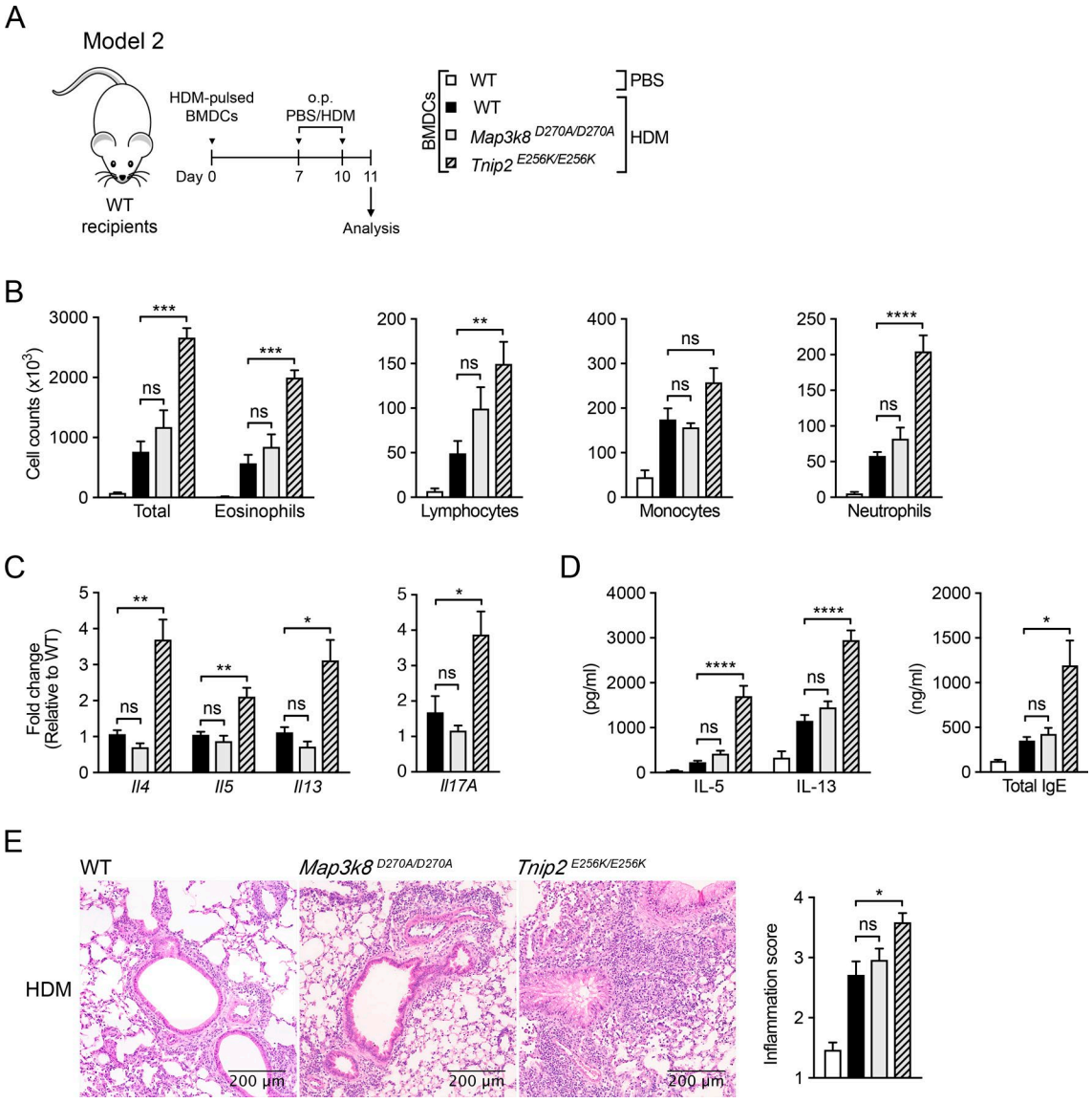

Figure S3. **HDM-pulsed Tnip2$^{E256K/E256K}$ BMDCs induce a severe airway allergic response. (A)** Schematic representation of the BMDC adoptive transfer model of HDM-induced airway allergic inflammation (Model 2). o.p., oropharyngeal. **(B)** Differential cell counts in BAL fluids from PBS- or HDM-challenged WT mice after adoptive transfer of HDM-pulsed WT, *Map3k8*$^{D270A/D270A}$, or *Tnip2*$^{E256K/E256K}$ BMDCs. **(C)** Cytokine mRNA expression levels in the lung, as assessed by qRT-PCR. **(D)** Total IgE levels in blood serum, IL-5, and IL-13 levels in BAL fluid, as assessed by ELISA. **(E)** H&E-stained lung sections (left panel) and inflammation scores (right panel) from PBS and HDM-challenged BMDC adoptively transferred mice. Data in panels B–E are shown as mean ± SEM and are pooled from three independent experiments (n = 9–11 mice/genotype). *, P < 0.05; **, P < 0.005; ***, P < 0.001; ****, P < 0.0001. Comparisons assessed by Kruskal-Wallis and Dunn-Bonferroni's post hoc test. ns, not significant.